ODA, M. (1985). *Géotechnique* **35**, No. 4, 483–495

Permeability tensor for discontinuous rock masses

M. ODA*

Rock masses, which commonly contain a large number of discontinuities, are treated as homogeneous, anisotropic porous media to formulate the corresponding permeability tensor. This has been successfully achieved by introducing a symmetric tensor (crack tensor) which depends only on the geometry of the related cracks (aperture, size and orientation). The principal directions associated with the symmetric crack tensor are coaxial with those of the permeability tensor. The first invariant of the crack tensor is proportional to the mean permeability, while the deviatoric part is related to the anisotropic permeability. These results are well supported by numerical experiments on the permeability of cracked media by Long, Remer, Wilson and Witherspoon. An actual rock mass (moderately jointed granite) was studied to see whether the crack tensor can be determined in situ. Stereology, based on geometrical statistics, provides a sound basis for determining the crack tensor in situ. The crack tensor is obtained by treating statistically the crack orientation data presented via a stereographic projection together with the detailed mapping of crack traces visible on rock exposures.

Des masses rocheuses, qui contiennent généralement un grand nombre de discontinuités, sont traitées comme des matières poreuses anisotropes homogènes pour formuler le tenseur de perméabilité correspondante. Ceci a été obtenu en introduisant un tenseur symétrique (tenseur de fissure) qui ne dépend que de la géometrie des fissures associées (ouverture, grandeur et orientation). Les directions principales associées avec le tenseur symétrique des fissures sont coaxiales avec celles du tenseur de perméabilité. Le premier invariant du tenseur des fissures est proportionnel à la perméabilité moyenne, tandis que la partie déviatorique est reliée à la perméabilité anisotrope. Ces résultats sont clairement confirmés par de nombreuses expériences sur la perméabilité des matières fissurées effectuées par Long, Remer, Wilson et Witherspoon. Une masse rocheuse (granit modérement fracturé) a été étudiée pour découvrir si on pouvait déterminer le tenseur des fissures en place. La stéréologie, basée sur la statistique géometrique, fournit une base valable pour determiner le tenseur des fissures en place. Le tenseur des fissures est obtenu par le traitement statistique des données de l'orientation des fissures présentées par projection stéréographique, accompagné du relevé detaillé des traces de fissures visibles sur les roches exposées.

KEYWORDS: anisotropy; permeability; rock mechanics; site investigation; water flow.

INTRODUCTION

Seepage of water sometimes exerts a dominant effect on the stability of engineering structures constructed on (or in) jointed rock masses. The uplift force by water pressure, for example, can cause serious damage to hydraulic fills (e.g. Müller, 1964). In recent years, engineers have been faced with more serious problems than ever. For example, very low flow rates can be a serious problem in the context of isolating radioactive waste buried in a rock mass.

Some experiments suggest that there is a marked difference between the permeabilities measured in the laboratory and in situ (e.g. Brace, 1980). This is true especially for crystalline rocks, and the difference is believed to be due to the presence of faults, joints and other planar discontinuities. In spite of the understanding that cracks are certainly major flow paths that are much more significant than those in the intact rock, they cannot be sampled adequately for laboratory measurements. Accordingly, a theoretical or numerical approach, in addition to field measurements, becomes of practical importance for evaluating the effect of discontinuities on the permeability; see, for example, Snow (1969), Parsons (1966), Caldwell (1972), Hudson & Pointe (1980), Long, Remer, Wilson & Witherspoon (1982) and Dienes (1982).

If a cracked rock mass can be assumed to be a homogeneous, anisotropic porous medium, it obeys Darcy's law in which the apparent seepage velocity $\bar{v}_i$ is related to the gradient $-\partial\phi/\partial x_i$ of total hydraulic head ϕ through a linking coefficient k_{ij} called the permeability tensor

$$\bar{v}_i = -\frac{g}{\nu} k_{ij} \frac{\partial \phi}{\partial x_j} = \frac{g}{\nu} k_{ij} J_j \qquad (1)$$

where g is the gravitational acceleration, ν is the kinematic viscosity and J_i is $-\partial\phi/\partial x_i$ (e.g. Scheidegger, 1957; Bear, 1972). It is not always certain that any rock mass can be simulated by an equivalent porous medium with a symmetric permeability tensor. However, the numerical study by Long *et al.* (1982) has suggested that a rock mass behaves more like a porous medium if

Discussion on this Paper closes on 1 April 1986. For further details see inside back cover.

* Saitama University.

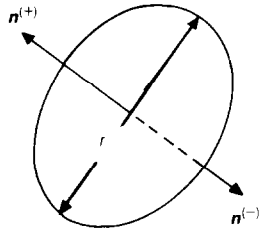

Fig. 1. Orientation of a crack

a sufficient number of discontinuities are present. In the following text, the word 'crack' has been used generically to describe a variety of discontinuity types which would occur in practice.

PERMEABILITY TENSOR

Cracks

Let us consider a cube of volume V as a flow region. It is homogeneously cut by $m^{(V)}$ cracks whose centres occur at random in the volume. Since there is little reliable information about the general shape of actual cracks, penny-shaped cracks with diameter r and aperture t are assumed here (e.g. Robertson, 1970). Then, each crack is associated with a void volume equal to $(\pi/4)r^2t$. The orientation of a crack is indicated by two unit normal vectors, $\boldsymbol{n}^{(+)}$ and $\boldsymbol{n}^{(-)}$, that are normal to the major plane (Fig. 1). It should be noted that $\boldsymbol{n}^{(+)}$ is parallel, but in the opposite direction, to $\boldsymbol{n}^{(-)}$. Here, $\boldsymbol{n}$ denotes both $\boldsymbol{n}^{(+)}$ and $\boldsymbol{n}^{(-)}$ and is oriented over the entire solid angle Ω corresponding to the surface of a unit sphere.

Impermeable matrix

A cracked rock mass with an impermeable matrix will be discussed first. Since water only flows through the cracks, the apparent flow velocity $\bar{v}_i$ is defined by

$$\bar{v}_i = \frac{1}{V}\int_V v_i \, dV = \frac{1}{V}\int_{V^{(c)}} v_i^{(c)} \, dV^{(c)} \qquad (2)$$

Here, $v_i^{(c)}$ is the local velocity in the cracks and $V^{(c)}$ is the volume associated with the cracks.

To use equation (2) further, attention is focused for the moment on $(\boldsymbol{n}, r, t)$ cracks characterized by the following. The unit vectors normal to the cracks are oriented inside a small solid angle $d\Omega$ around $\boldsymbol{n}$, and the diameters and the apertures range from r to $r+dr$ and from t to $t+dt$ respectively. Now, the probability density function $E(\boldsymbol{n}, r, t)$ is introduced in such a way that $2E(\boldsymbol{n}, r, t)\, d\Omega\, dr\, dt$ gives the probability of $(\boldsymbol{n}, r, t)$ cracks. It satisfies

$$\int_0^\infty \int_0^\infty \int_{\Omega/2} 2E(\boldsymbol{n}, r, t)\, d\Omega\, dr\, dt = \int_0^\infty \int_0^\infty \int_{\Omega} E(\boldsymbol{n}, r, t)\, d\Omega\, dr\, dt = 1 \qquad (3)$$

where $\Omega/2$ is the half of Ω corresponding to the surface of a hemisphere. (Two points should be noted here with regard to equation (3). Firstly the limits of infinity must be replaced by the maximum sizes of r and t if cracks in an elementary volume V are considered. Henceforth, infinity symbols are used merely for convenience. Secondly each crack produces two unit normal vectors $\boldsymbol{n}^{(+)}$ and $\boldsymbol{n}^{(-)}$ with opposite directions. Then, $E(\boldsymbol{n}, r, t)\, d\Omega\, dr\, dt$ gives the probability of the unit normals of $(\boldsymbol{n}, r, t)$ cracks, not of the cracks themselves. In this case, the function $E(\boldsymbol{n}, r, t)$ is defined over the entire solid angle Ω. However, $2E(\boldsymbol{n}, r, t)\, d\Omega\, dr\, dt$ gives the probability of $(\boldsymbol{n}, r, t)$ cracks where the function is only defined over the half solid angle $\Omega/2$.) Bearing in mind that the centres of cracks occur at random in the flow region, it can be said that the crack geometry is completely specified by the density function plus the number of cracks. It should also be noted that $E(\boldsymbol{n}, r, t) = E(-\boldsymbol{n}, r, t)$, since $\boldsymbol{n}$ denotes $\boldsymbol{n}^{(+)}$ and $\boldsymbol{n}^{(-)}$.

Let dN be a number of $(\boldsymbol{n}, r, t)$ cracks whose centres are located inside the flow region of volume V. To estimate the number, the probability of $(\boldsymbol{n}, r, t)$ cracks is multiplied by the total number $m^{(V)}$

$$dN = 2m^{(V)} E(\boldsymbol{n}, r, t)\, d\Omega\, dr\, dt \qquad (4)$$

Since each $(\boldsymbol{n}, r, t)$ crack produces a void volume equal to $(\pi/4)r^2t$, the total void volume $dV^{(c)}$ associated with the $(\boldsymbol{n}, r, t)$ cracks is given by

$$dV^{(c)} = \frac{\pi r^2 t}{4} dN = \frac{\pi m^{(V)}}{2} r^2 t\, E(\boldsymbol{n}, r, t)\, d\Omega\, dr\, dt \qquad (5)$$

Next consider the flow velocity suitable for $(\boldsymbol{n}, r, t)$ cracks. The flow region considered here consists of two constant head boundaries ($\phi_1 > \phi_2$) and four boundaries with the same linear variation in head from ϕ_1 to ϕ_2, so that the gradient $\boldsymbol{J}$ is given by

$$\boldsymbol{J} = \frac{\phi_1 - \phi_2}{L}\boldsymbol{p} \qquad (6)$$

where L is the distance between the two constant head boundaries and $\boldsymbol{p}$ is a unit vector pointing to $\boldsymbol{J}$ (Fig. 2). ($\boldsymbol{J}$ is called the field

gradient by Snow (1969).) The distribution of the head inside the flow region depends entirely on the hydraulic response of the crack system. Here, it is assumed that the head linearly decreases, i.e. the field gradient $\boldsymbol{J}$ is uniform over the whole flow region. This assumption has been supported by Long *et al.* (1982) on the basis of analyses on the permeability of cracked media. It is worthy of note, however, that this assumption is acceptable only if the body contains a sufficient number of cracks.

Now, let $\boldsymbol{J}^{(c)}$ be a component of $\boldsymbol{J}$ projected on an $(\boldsymbol{n}, r, t)$ crack (Fig. 3)

$$\boldsymbol{J}^{(c)} = \boldsymbol{J} - (\boldsymbol{n} \cdot \boldsymbol{J})\boldsymbol{n} \tag{7a}$$

or alternatively

$$J_i^{(c)} = (\delta_{ij} - n_i n_j) J_j \tag{7b}$$

where δ_{ij} is the Kronecker delta and n_i and J_i respectively are components of $\boldsymbol{n}$ and $\boldsymbol{J}$ projected on the orthogonal reference axes x_i $(i = 1, 2, 3)$. (The summation convention is adopted if any subscript appears twice. This is not the case, however, when superscripts are in parentheses.) If the crack extends indefinitely, the water movement can be idealized by laminar flow between parallel planar plates with an aperture t. It has the following mean velocity $v_i^{(c)}$

$$v_i^{(c)} = \frac{1}{12} \frac{g}{\nu} t^2 J_i^{(c)} \tag{8}$$

Equation (8) has been employed where it is intended to develop a mathematical expression for the permeability tensor of rock masses (e.g. Snow, 1969).

Witherspoon, Wang, Imai & Gale (1980) have measured the effective permeabilities of artificial cracks made in basalt, granite and marble stressed up to 20 MPa and have shown that equation (8) is still valid for apertures ranging from 250 μm down to 4 μm. However, it may not be correct to assume in general that actual cracks extend indefinitely. Rather, it may be more appropriate for $(\boldsymbol{n}, r, t)$ cracks to have the following flow velocity

$$v_i^{(c)} = \lambda \frac{g}{\nu} t^2 J_i^{(c)} \tag{9}$$

where λ is a dimensionless constant with the restriction $0 < \lambda \leq 1/12$. The constant approaches 1/12 with increasing size of the related cracks.

Substituting $J_i^{(c)}$ of equation (7) in equation (9), the apparent velocity associated with $(\boldsymbol{n}, r, t)$ cracks is finally written as

$$v_i^{(c)} = \lambda \frac{g}{\nu} t^2 (\delta_{ij} - n_i n_j) J_j \tag{10}$$

Using equations (5) and (10), equation (2) becomes

$$\begin{aligned} \bar{v}_i &= \frac{1}{V} \int_{V^{(c)}} v_i^{(c)} \, \mathrm{d}V^{(c)} \\ &= \lambda \frac{g}{\nu} \left[\frac{\pi \rho}{4} \int_0^\infty \int_0^\infty \int_\Omega r^2 t^3 (\delta_{ij} - n_i n_j) \right. \\ &\quad \left. \times E(\boldsymbol{n}, r, t) \, \mathrm{d}\Omega \, \mathrm{d}r \, \mathrm{d}t \right] J_j \end{aligned} \tag{11}$$

where ρ is the volume density of cracks defined by

$$\rho = \frac{m^{(V)}}{V} \tag{12}$$

The integration is carried out over all cracks in the flow region.

A comparison between equation (11) and Darcy's law (equation (1)) leads to an equivalent permeability tensor $k_{ij}^{(c)}$ responsible for the

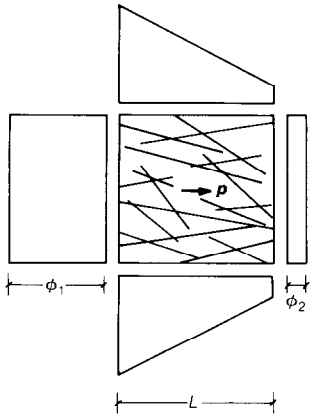

Fig. 2. Cubical flow region with two constant head boundaries ($\phi_1 > \phi_2$) and four boundaries with a linear variation in head from ϕ_1 to ϕ_2 (two-dimensional drawing)

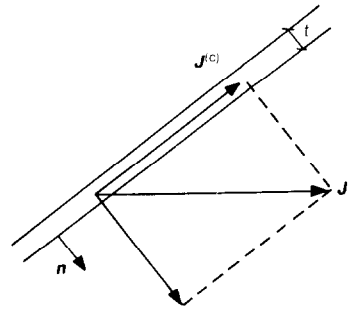

Fig. 3. Hydraulic gradient $J_i^{(c)}$ along an $(\boldsymbol{n}, r, t)$ crack

crack system, as follows

$$k_{ij}^{(c)} = \lambda (P_{kk}\,\delta_{ij} - P_{ij}) \tag{13}$$

where

$$P_{ij} = \frac{\pi\rho}{4}\int_0^\infty \int_0^\infty \int_\Omega r^2 t^3 n_i n_j\, \mathrm{E}(\boldsymbol{n}, r, t)\, \mathrm{d}\Omega\, \mathrm{d}r\, \mathrm{d}t \tag{14}$$

and

$$P_{kk} = P_{11} + P_{22} + P_{33} \tag{15}$$

The notation P_{ij}, which is tentatively called the 'crack tensor', is a symmetric, second-rank tensor relating only to the crack geometry, i.e. to the crack shape, crack size, aperture and orientation.

Equation (13) is formulated on the basic assumption that the flow region is fully divided by cracks so that there are many flow paths in it. The final equation produces a non-zero permeability even when P_{ij} becomes negligibly small. In reality, however, the flow region may become impermeable because the connectivity is completely lost in spite of the presence of cracks. To correct this shortcoming, the following modification is given: the crack tensor P_{ij} is decreased in such a way that it is multiplied by a positive scalar α that is less than unity. A threshold value can be observed at $\alpha = \alpha_0$ below which the region becomes practically impermeable because of the complete loss of the connectivity between cracks. Then, a correction term a_{ij} is introduced such that when $\alpha > \alpha_0$

$$k_{ij}^{(c)} = \lambda (P_{kk}\,\delta_{ij} - P_{ij}) + a_{ij} \tag{16a}$$

and when $0 < \alpha \leqslant \alpha_0$

$$k_{ij}^{(c)} = 0 \tag{16b}$$

Since $k_{ij}^{(c)} = 0$ at $\alpha = \alpha_0$, the correction term becomes

$$a_{ij} = -\lambda\alpha_0 (P_{kk}\,\delta_{ij} - P_{ij}) \tag{17}$$

Substituting this in equation (16), the permeability tensor is finally given by

$$\begin{aligned} k_{ij}^{(c)} &= \lambda (1-\alpha_0)(P_{kk}\,\delta_{ij} - P_{ij}) \\ &= \lambda (\bar{P}_{kk}\,\delta_{ij} - \bar{P}_{ij}) \end{aligned} \tag{18}$$

where $\bar{P}_{ij} = P_{ij} - P_{ij}^{(0)}$ and $P_{ij}^{(0)} = \alpha_0 P_{ij}$. Here, $P_{ij}^{(0)}$ gives a threshold, in the sense that the mass becomes impermeable if the corresponding crack tensor is less than $P_{ij}^{(0)}$. In such a case that the flow region is fully divided by many large cracks, $P_{ij}^{(0)}$ can be set to zero because it becomes very small compared with P_{ij}, and therefore equation (13) with $\lambda = 1/12$ is used. Fortunately, this may be a common case in practice since most crystalline rocks are seriously damaged by many cracks. In fact, full connectivity between cracks is commonly observed in situ.

Permeable matrix

In certain sandstones and shales, flow through the permeable matrix cannot be disregarded (Brace, 1980). In this case, equation (2) is written in the form

$$\begin{aligned} \bar{v}_i &= \frac{1}{V}\int_V v_i\, \mathrm{d}V \\ &= \frac{1}{V}\left(\int_{V^{(\mathrm{m})}} v_i^{(\mathrm{m})}\, \mathrm{d}V^{(\mathrm{m})} + \int_{V^{(c)}} v_i^{(c)}\, \mathrm{d}V^{(c)}\right) \end{aligned} \tag{19}$$

where the superscript m denotes matrix. (Equation (19) corresponds to an assumption that the non-steady interaction between the double porosities can be neglected.) Since the permeable matrix behaves like an ideal porous medium, there must be a complementary permeability tensor $k_{ij}^{(\mathrm{m})}$. The void volume $V^{(c)}$ associated with the cracks is usually so small that $V^{(\mathrm{m})}$ is nearly equal to V. Then, equation (19) becomes

$$\begin{aligned} \bar{v}_i &= \frac{1}{V}\left(\int_V v_i^{(\mathrm{m})}\, \mathrm{d}V + \int_{V^{(c)}} v_i^{(c)}\, \mathrm{d}V^{(c)}\right) \\ &= \frac{g}{\nu}(k_{ij}^{(\mathrm{m})} + k_{ij}^{(c)}) J_j \end{aligned} \tag{20}$$

Comments on the permeability tensor

Before discussing the utility of equations (13) and (18), it is important to point out the following characteristics.

(*a*) The tensors $k_{ij}^{(c)}$ and P_{ij} are both symmetric, i.e. $k_{ij}^{(c)} = k_{ji}^{(c)}$ and $P_{ij} = P_{ji}$. Therefore their principal values in the corresponding principal directions can always be determined. Let x_1', x_2' and x_3' be the major, intermediate and minor principal axes of P_{ij}. With reference to the principal axes, these tensors can both be diagonalized in matrix form as follows

$$P_{ij} = \begin{bmatrix} P_1 & 0 & 0 \\ 0 & P_2 & 0 \\ 0 & 0 & P_3 \end{bmatrix}$$

$$k_{ij}^{(c)} = \begin{bmatrix} k_1^{(c)} & 0 & 0 \\ 0 & k_2^{(c)} & 0 \\ 0 & 0 & k_3^{(c)} \end{bmatrix} \tag{21}$$

Since $k_{ij}^{(c)}$ is a unique function of P_{ij} (or $\bar{P}_{ij}$), its principal axes are coaxial with those of the crack tensors, with the major permeability in the minor principal direction of P_{ij} ($k_1^{(c)} \leqslant k_2^{(c)} \leqslant k_3^{(c)}$).

(*b*) By setting $i = j$ in equation (18)

$$k_{ii}^{(c)} = 2\lambda \bar{P}_{ii} = 2\lambda (P_{ii} - P_{ii}^{(0)}) \tag{22}$$

(*c*) For the two-dimensional case equation (22)

is rewritten as

$$k_{ii}^{(c)} = \lambda \bar{P}_{ii} = \lambda (P_{ii} - P_{ii}^{(0)}) \tag{23}$$

Let x_1' and x_2' be the major and minor axes of P_{ij} respectively. With reference to these axes equation (18) is transformed to

$$\begin{bmatrix} k_1^{(c)} \\ k_2^{(c)} \end{bmatrix} = \lambda (1 - \alpha_0) \begin{bmatrix} P_2 \\ P_1 \end{bmatrix} \tag{24}$$

which leads to

$$\begin{bmatrix} k_1^{(c)} \\ \overline{k_2^{(c)}} \end{bmatrix} \begin{bmatrix} P_1 \\ \overline{P_2} \end{bmatrix} = 1 \tag{25}$$

These characteristics must be carefully examined in the light of experiments to see whether the theory can provide a sound basis for estimating the permeability that is suitable for a given crack system.

NUMERICAL EXPERIMENTS RELATING TO THE PERMEABILITY TENSOR

If it is possible, the theory must be verified experimentally. Unfortunately, however, there are no experimental data available at present. Instead, numerical experiments done by Long *et al.* (1982) can be used to provide an example supporting the present theory.

General remarks

Let $K^{(\mathbf{p})}$ be the permeability in the direction $\boldsymbol{p}$ (directional permeability), which is parallel to a field gradient $\boldsymbol{J}$, and let J be the magnitude of $\boldsymbol{J}$ ($\boldsymbol{J} = J\boldsymbol{p}$). Then, $K^{(\mathbf{p})}$ must satisfy (e.g. Bear, 1972)

$$\bar{v}_i p_i = \frac{g}{\nu} K^{(\mathbf{p})} J \tag{26}$$

Substituting Darcy's law, equation (26) becomes

$$K^{(\mathbf{p})} = k_{ij} p_i p_j \tag{27}$$

Once the permeability tensor has been fixed, equation (27) makes it possible to calculate the directional permeability in any direction. However, a general method is sometimes needed to calculate the permeability tensor from the directional permeabilities $\underline{K}^{(\mathbf{p}^{(k)})}$ which are experimentally (or numerically) determined in various directions $\boldsymbol{p}^{(k)}$ ($k = 1, 2, \ldots, m$). This problem has been solved by Kanatani (1984), who suggested the following equation for two-dimensional cases

$$\bar{k}_{ij}^{(c)} = \frac{2}{\pi} \left(\sum_{k=1}^{m} \underline{K}^{(\mathbf{p}^{(k)})} p_i^{(k)} p_j^{(k)} - \frac{1}{4} \delta_{ij} \sum_{k=1}^{m} \underline{K}^{(\mathbf{p}^{(k)})} \right) \quad (i, j = 1, 2) \tag{28}$$

Using the tensor $\bar{k}_{ij}^{(c)}$ for k_{ij} in equation (27), the directional permeability $\bar{K}^{(\mathbf{p})}$ is again calculated. It should be noted that equation (28) is formulated to minimize the sum of the squares of the errors, $(\bar{K}^{(\mathbf{p})} - \underline{K}^{(\mathbf{p})})^2$.

Numerical analyses by Long et al. (1982)

Long *et al.* (1982) have numerically determined the directional permeabilities $\underline{K}^{(\mathbf{p}^{(k)})}$ ($k = 1, 2, \ldots, m$) of two-dimensional crack systems. In their simulation, two-dimensional cracks are treated as line elements with flux related to aperture by the cubic law, and the intact rock is assumed to be impermeable. The flow region consists of two constant head boundaries ($\phi_1 > \phi_2$) and two boundaries with the same linear variation in head from ϕ_1 to ϕ_2. For each crack system, the direction of the field gradient was rotated to examine the change in the directional permeability $\underline{K}^{(\mathbf{p}^{(k)})}$.

Four crack systems (A–D) are taken from the paper by Long *et al.* and are reproduced in Figs 4–7, together with polar diagrams showing the variation in the directional permeability. The cracks consist of two sets, set 1 and set 2, with uniform characteristics as summarized in Table 1. Since all the information relating to the crack geometry is available, the additive form, rather than the integral form, of equation (14) can be used to determine the crack tensors. The component P_{12}, for example, is

$$P_{12} = \sum_{k=1}^{m^{(V)}} Tr^{(k)} (t^{(k)})^3 \cos\theta^{(k)} \sin\theta^{(k)} \tag{29}$$

where the superscript k denotes the kth crack among $m^{(V)}$ cracks, $\theta^{(k)}$ is the angle of inclination of $\boldsymbol{n}^{(k)}$ to the reference axis x_1 and T is the depth of cracks. (Since T does not have an effect on the result, it is set to unity. It should also be noted that n_i in equation (14) is a direction cosine of $\boldsymbol{n}$ with reference to a selected axis x_i. Using the angle $\theta^{(k)}$, therefore, $n_1 n_2$ is given by $\cos\theta^{(k)} \sin\theta^{(k)}$.) With respect to the reference axes x_1 and x_2, the crack tensors $P_{ij}^{(A)}$, $P_{ij}^{(B)}$, $P_{ij}^{(C)}$ and $P_{ij}^{(D)}$ are given in matrix form as

$$[P_{ij}^{(A)}] = \begin{bmatrix} P_{11} & P_{12} \\ P_{21} & P_{22} \end{bmatrix} = \begin{bmatrix} 2{\cdot}70 & -1{\cdot}65 \\ -1{\cdot}65 & 1{\cdot}12 \end{bmatrix} \times 10^{-9}\ \mathrm{cm}^2$$

$$[P_{ij}^{(B)}] = \begin{bmatrix} 4{\cdot}20 & -2{\cdot}57 \\ -2{\cdot}57 & 1{\cdot}73 \end{bmatrix} \times 10^{-9}\ \mathrm{cm}^2 \tag{30a}$$

$$[P_{ij}^{(C)}] = \begin{bmatrix} 5{\cdot}58 & -3{\cdot}44 \\ -3{\cdot}44 & 2{\cdot}35 \end{bmatrix} \times 10^{-9}\ \mathrm{cm}^2$$

$$[P_{ij}^{(D)}] = \begin{bmatrix} 3{\cdot}75 & -2{\cdot}63 \\ -2{\cdot}63 & 1{\cdot}57 \end{bmatrix} \times 10^{-9}\ \mathrm{cm}^2$$

Let x_1' and x_2' be the major and minor principal axes of P_{ij} respectively. The principal axes, calculated from equation (30a), are shown in Figs 4–7 with the following principal values

$$[P_{ij}^{(A)}]=\begin{bmatrix}P_1 & 0\\ 0 & P_2\end{bmatrix}=\begin{bmatrix}37{\cdot}4 & 0\\ 0 & 0{\cdot}773\end{bmatrix}\times 10^{-10}\,\mathrm{cm}^2$$

$$[P_{ij}^{(B)}]=\begin{bmatrix}58{\cdot}1 & 0\\ 0 & 1{\cdot}15\end{bmatrix}\times 10^{-10}\,\mathrm{cm}^2 \qquad (30b)$$

$$[P_{ij}^{(C)}]=\begin{bmatrix}77{\cdot}8 & 0\\ 0 & 1{\cdot}72\end{bmatrix}\times 10^{-10}\,\mathrm{cm}^2$$

$$[P_{ij}^{(D)}]=\begin{bmatrix}49{\cdot}9 & 0\\ 0 & 3{\cdot}61\end{bmatrix}\times 10^{-10}\,\mathrm{cm}^2$$

Three kinds of directional permeability are distinguished in the polar diagrams of Figs 4–7: $\underline{K}^{(p)}$ (full curve), the directional permeability determined from the numerical analyses by Long *et al.* (1982); $\bar{K}^{(p)}$ (broken curve), the directional permeability calculated by substituting the estimated permeability tensor $\bar{k}_{ij}^{(c)}$ in equation (27) (the corresponding principal axes are projected in Figs 4–7 as $x_1°$(minor) and $x_2°$(major)); $K^{(p)}$ (dotted curve), the directional permeability calculated by substituting the crack tensor of equation (30) in equation (18) on the assumption that $\alpha_0 = 0$ and $\lambda = 1/12$. The corresponding principal axes exactly coincide with the principal axes of the crack tensor, x_1'(major) and x_2'(minor).

A comparison of these directional permeabilities leads to the following observations.

(*a*) The crack system can be idealized by a hydraulically equivalent porous medium if the variation in $\bar{K}^{(p)}$ (broken curve) accords with that of $\underline{K}^{(p)}$ (full curve). Such an accordance becomes manifest when the crack density is increased from sample A to sample C, and also when the orientations are random (sample D) rather than constant (sample B). This result may be able to explain whether the connectivity between cracks is adequately taken into account.

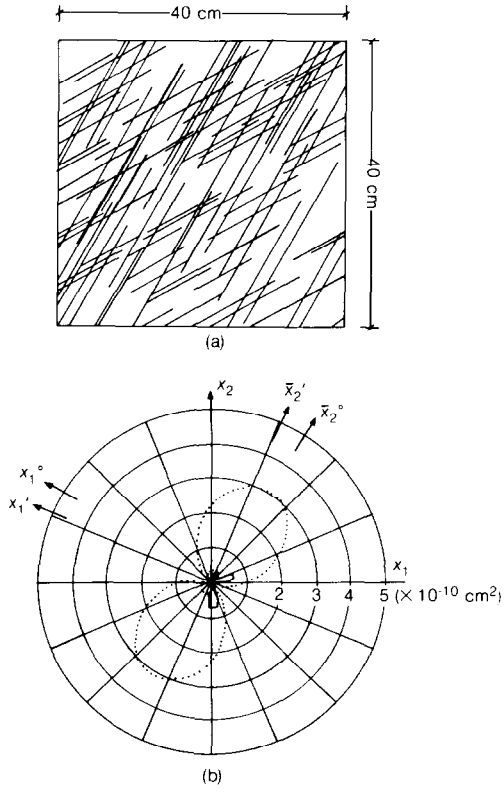

Fig. 4. (a) Crack system of sample A and (b) the corresponding directional permeabilities ($\underline{K}^{(p)}$ (full curve) is the directional permeability taken from Long *et al.* (1982); $\bar{K}^{(p)}$ (broken curve) is the directional permeability calculated from $k_{ij}^{(c)}$; $K^{(p)}$ (dotted curve) is the directional permeability derived from theory)

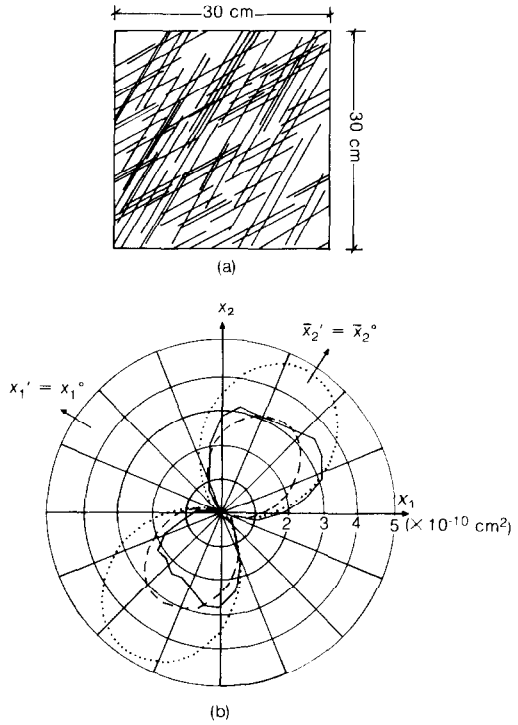

Fig. 5. (a) Crack system of sample B and (b) the corresponding directional permeabilities $\underline{K}^{(p)}$ (full curve), $\bar{K}^{(p)}$ (broken curve) and $K^{(p)}$ (dotted curve)

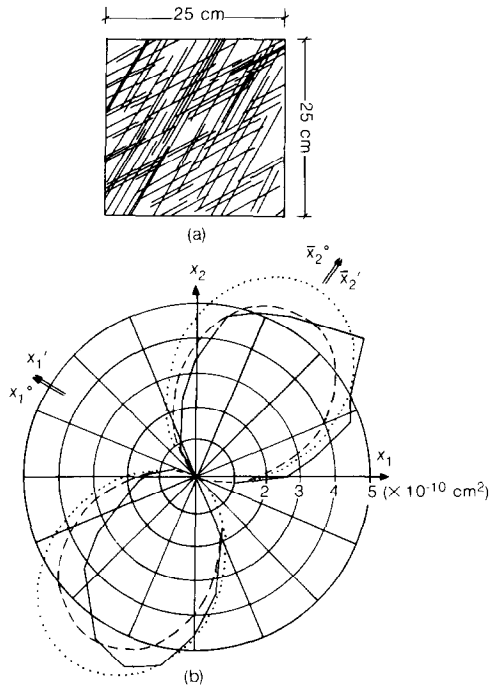

Fig. 6. (a) Crack system of sample C and (b) the corresponding directional permeabilities $\underline{K}^{(p)}$ (full curve), $\bar{K}^{(p)}$ (broken curve) and $K^{(p)}$ (dotted curve)

(*b*) If the flow region is well divided by cracks, as for samples C and D, the substitution of $\alpha_0 = 0$ and $\lambda = 1/12$ in equation (18) provides a reasonable prediction of the directional permeability which follows the numerically obtained permeabilities ($K^{(p)} \approx \bar{K}^{(p)}$). For sample A which is practically impermeable, however, $K^{(p)}$ differs completely from $\underline{K}^{(p)}$. It should be noted, however, that the dotted curves ($K^{(p)}$) can be fitted to the broken curves ($\bar{K}^{(p)}$) if λ is set as 1/100 for sample A, 1/18·4 for sample B, 1/13·9 for sample C and 1/12·8 for sample D.

(*c*) There is exact agreement between the principal axes x_i' of the crack tensor and the principal axes x_i° of the permeability tensor. This coaxiality is in good accordance with the theoretical prediction.

Table 1. Crack data for samples A, B and C

Set	Uniform orientation: deg	Uniform length: cm	Uniform aperture: cm	Number of fractures
1	30	10	0·001	60
2	60	20	0·002	40

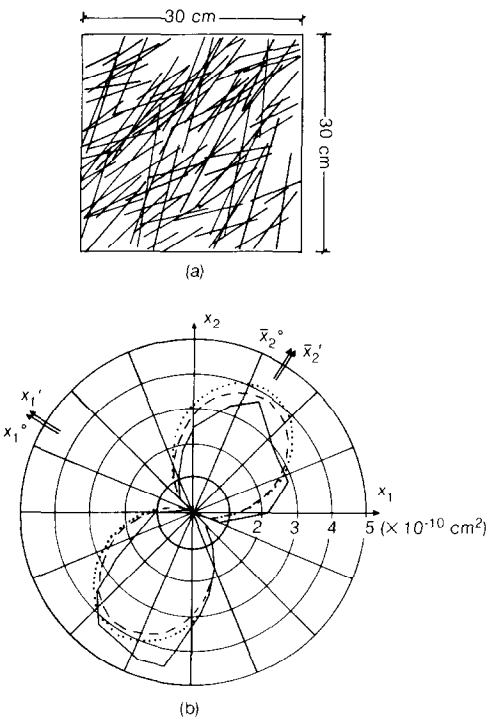

Fig. 7. (a) Crack system of sample D with the same, but dispersed, cracks as sample B and (b) the corresponding directional permeabilities $\underline{K}^{(p)}$ (full curve), $\bar{K}^{(p)}$ (broken curve) and $K^{(p)}$ (dotted curve)

One more example is taken from the paper by Long *et al.* (1982) and is reproduced in Fig. 8. In this case, the cracks consist of two perpendicular sets with a common aperture ($t = t_0$) and a common crack length. The flow region has been enlarged to see whether the size has a real influence on the permeability (Fig. 8). It has been clearly shown that the variation in the directional permeability $\underline{K}^{(p)}$ differs from that of

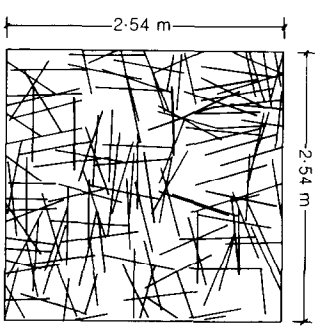

Fig. 8. Crack system composed of two sets of cracks (Long *et al.*, 1982)

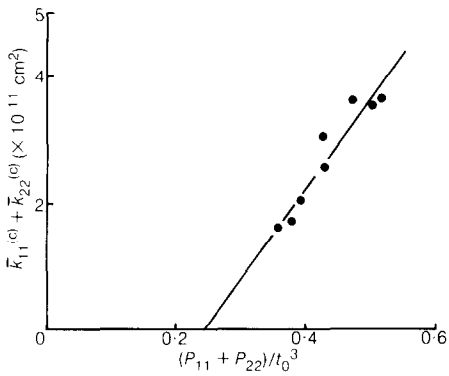

Fig. 9. Linear relation between the trace of the permeability tensor and the trace of the crack tensor

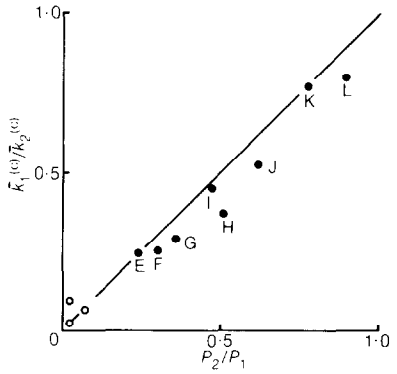

Fig. 10. Relation between $\bar{k}_1^{(c)}/\bar{k}_2^{(c)}$ (the anisotropy in the permeability) and P_2/P_1 (the anisotropy in the crack tensor)

anisotropic porous media until the flow region is enlarged beyond a critical size, i.e. a crack system cannot be replaced by a hydraulically equivalent porous medium unless there is a sufficient number of cracks in the representative elementary volume. Here, the permeability tensors $\bar{k}_{ij}^{(c)}$ for the regions larger than the critical size are discussed, with the results summarized in Figs 9 and 10.

In Fig. 9, the trace of the permeability tensor $\bar{k}_{ij}^{(c)}$ is related to the trace of the corresponding crack tensor P_{ii} divided by the cube of the aperture t_0. These data can be fitted to the regression line

$$\bar{k}_{ii}^{(c)} = \bar{\lambda}\left(\frac{P_{ii}}{t_0^3} - \frac{P_{ii}^{(0)}}{t_0^3}\right) \tag{31}$$

where $\bar{\lambda}$ is a tangent to the regression line. The complete accordance between equation (31) and equation (23) when λ is set to $\bar{\lambda}/t_0^3$ should be noted.

Let $\bar{k}_1^{(c)}$ and $\bar{k}_2^{(c)}$ be the minor and major principal permeabilities, and P_1 and P_2 be the major and minor principal values of the crack tensor respectively. In Fig. 10, the anisotropy of the permeability represented by the ratio $\bar{k}_1^{(c)}/\bar{k}_2^{(c)}$ is shown as a function of the anisotropy of the crack geometry represented by the ratio P_2/P_1. (The data for samples B, C and D in Figs 5–7 are also included in the figure.) The result supports equation (25), giving the relation $(\bar{k}_1^{(c)}/\bar{k}_2^{(c)})(P_1/P_2) = 1$.

In conclusion therefore the numerical experiments by Long *et al.* (1982) can be said to support the permeability tensor in terms of the crack tensor.

DETERMINATION OF THE CRACK TENSOR

General consideration

In the previous section, the permeability tensor has been successfully formulated in terms of the crack tensor. The next problem to be solved is whether there is a reliable method to predict the crack tensor for rock masses in situ. There is no difficulty if all the information concerning cracks is available beforehand. Since this is not usually the case in practice, a method using the geometrical probability (stereology) will be discussed here.

One assumption adopted here is that the random variables $\boldsymbol{n}$, r and t are statistically independent of one another, i.e.

$$\mathrm{E}(\boldsymbol{n}, r, t) = \mathrm{E}(\boldsymbol{n})\mathrm{f}(r)\mathrm{g}(t) \tag{32}$$

where $\mathrm{E}(\boldsymbol{n})$, $\mathrm{f}(r)$ and $\mathrm{g}(t)$ are the density functions of $\boldsymbol{n}$, r and t respectively. If equation (32) does not hold, cracks must be classified into a few homogeneous groups for each of which equation (32) does hold. In such a case, the crack tensors are considered individually first and are summed afterwards.

The orientation of cracks is commonly represented by contour lines of $\boldsymbol{n}$ vectors on Schmidt's equal area net. Each contour line is labelled by the percentage concentration of $\boldsymbol{n}$ vectors per unit per cent area (e.g. Turner & Weiss, 1963; Hoek & Brown, 1980). It is easy to prove that the percentage of each contour line has the same meaning as the contour of $\mathrm{E}(\boldsymbol{n})$ if it is divided by 4π. Accordingly, the conventional field survey supplies the density function $\mathrm{E}(\boldsymbol{n})$ (see Appendix 1). Great care must be paid to avoid biased sampling when crack data are obtained. However, it is very difficult to obtain reliable data on the density functions $\mathrm{f}(r)$ and $\mathrm{g}(t)$. Time-consuming work is necessary, especially for measuring the crack apertures in situ (e.g. Snow, 1968). To overcome the difficulty, one more assumption is adopted here, i.e. either the aperture is constant ($t = t_0$), or it is proportional to the crack size ($t = cr$).

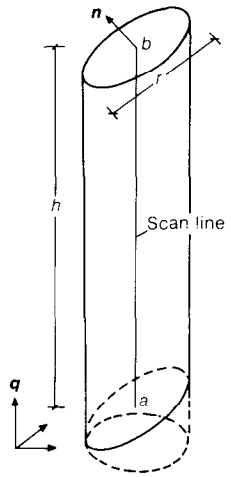

Fig. 11. Column extending parallel to a unit vector q whose upper and lower planes consist of (n, r, t) cracks

Crack tensor $(t = t_0)$

In the rather special case that the aperture is constant irrespective of the crack size, then the crack tensor of equation (14) becomes

$$P_{ij} = t_0^3 \frac{\pi\rho}{4}\int_0^\infty r^2 f(r)\,dr \int_\Omega n_i n_j E(\boldsymbol{n})\,d\Omega = \frac{\pi\rho t_0^3}{4}\langle r^2\rangle N_{ij} \tag{33}$$

where

$$N_{ij} = \int_\Omega n_i n_j\, E(\boldsymbol{n})\,d\Omega \tag{34}$$

is a symmetric, second-rank tensor calculated from the density function $E(\boldsymbol{n})$ only, and

$$\langle r^n\rangle = \int_0^\infty r^n f(r)\,dr \quad (n = 1, 2, \ldots) \tag{35}$$

is the nth moment of r.

To deal with equation (33) further, a straight scan line ab (length h) is set in the rock mass parallel to a unit vector $\boldsymbol{q}$ (Fig. 11). A column with the following characteristics is considered. The central axis coincides with the scan line. The upper and lower planes consist of $(\boldsymbol{n}, r, t)$ cracks so that the cross-sectional area is $(1/4)\pi r^2(\boldsymbol{n}\cdot\boldsymbol{q})$ (the area of an $(\boldsymbol{n}, r, t)$ crack projected on the plane perpendicular to $\boldsymbol{q}$). It is easily seen that any $(\boldsymbol{n}, r, t)$ crack must cross the scan line if the centre is placed just inside the column.

The length h of the scan line is so long that there are many cracks inside the volume V. It should be noted that multiplying the volume by ρ results in the total number of the cracks whose centres are located inside the column

$$\rho V_0 = \frac{\pi\rho}{4} h r^2 (\boldsymbol{n}\cdot\boldsymbol{q}) \tag{36}$$

If it is further multiplied by the probability of $(\boldsymbol{n}, r, t)$ cracks, it becomes the number $dN^{(\boldsymbol{q})}$ of $(\boldsymbol{n}, r, t)$ cracks whose centres are located inside the volume

$$dN^{(\boldsymbol{q})} = \frac{\pi\rho}{4} h r^2 |\boldsymbol{n}\cdot\boldsymbol{q}|\, 2E(\boldsymbol{n})\, f(r)\,d\Omega\,dr \tag{37}$$

$dN^{(\boldsymbol{q})}$ corresponds to the number of $(\boldsymbol{n}, r, t)$ cracks crossed by the scan line. To count all the cracks crossed by the scan line, equation (37) must be integrated over $\Omega/2$ and $0 \leqslant r < \infty$. It results in

$$\frac{N^{(\boldsymbol{q})}}{h} = \frac{\pi\rho}{4}\int_0^\infty r^2 f(r)\,dr \int_{\Omega/2} |\boldsymbol{n}\cdot\boldsymbol{q}|\, 2E(\boldsymbol{n})\,d\Omega = \frac{\pi\rho}{4}\langle r^2\rangle\langle|\boldsymbol{n}\cdot\boldsymbol{q}|\rangle \tag{38}$$

where

$$\langle|\boldsymbol{n}\cdot\boldsymbol{q}|\rangle = \int_\Omega |\boldsymbol{n}\cdot\boldsymbol{q}|\, E(\boldsymbol{n})\,d\Omega \tag{39}$$

is a scalar quantity calculated from the density function $E(\boldsymbol{n})$. Substituting equation (38) in equation (33), the crack tensor is finally given by

$$P_{ij} = \left(\frac{t_0^3 N^{(\boldsymbol{q})}/h}{\langle|\boldsymbol{n}\cdot\boldsymbol{q}|\rangle}\right) N_{ij} \tag{40}$$

Here, $N^{(\boldsymbol{q})}/h$ is the number of cracks crossed by unit length of the scan line in the direction $\boldsymbol{q}$, and $\langle|\boldsymbol{n}\cdot\boldsymbol{q}|\rangle$ is a correction factor with respect to the selected direction $\boldsymbol{q}$, i.e. $N^{(\boldsymbol{q})}/h$ divided by $\langle|\boldsymbol{n}\cdot\boldsymbol{q}|\rangle$ must be constant irrespective of the direction $\boldsymbol{q}$.

Crack tensor $(t = cr)$

It sometimes happens that a larger crack has a wider aperture. A possible assumption is therefore that the aperture is proportional to the size $(t = cr)$. (If a more elaborate relation is obtained in future, the following derivation can be slightly modified without difficulty.) Using $t = cr$, then the crack tensor is given by

$$P_{ij} = \frac{\pi\rho c^3}{4}\langle r^5\rangle N_{ij} \tag{41}$$

Actual cracks are observed as trace lines on exposures. Let $\psi(l)$ be a probability density function for the distribution of trace lengths l. The stereological study by Oda (1983, 1984) has proved that $\psi(l)$ is uniquely determined, not dependent on the orientation of the observed

wall, if $\boldsymbol{n}$ is a statistically independent variable of r. Furthermore, the nth moment of l is related to the moments of r as follows (see also Kendall & Moran, 1963)

$$\langle l^n \rangle = \frac{\langle r^{n+1} \rangle}{\langle r \rangle} \int_0^{\pi/2} \sin^{n+1} \theta \, \mathrm{d}\theta \tag{42}$$

where

$$\langle l^n \rangle = \int_0^{\infty} l^n \psi(l) \, \mathrm{d}l \tag{43}$$

Using equation (42), together with equation (38), $\langle r^5 \rangle$ becomes

$$\langle r^5 \rangle = \frac{15}{8} \langle l^4 \rangle \langle r \rangle = \frac{15\pi}{32} \frac{\langle l^4 \rangle}{\langle l \rangle} \langle r^2 \rangle = \frac{15}{8} \frac{\langle l^4 \rangle (N^{(q)}/h)}{\rho \langle l \rangle \langle |\boldsymbol{n} \cdot \boldsymbol{q}| \rangle} \tag{44}$$

Substituting this in equation (40), the crack tensor is finally given by

$$P_{ij} = \frac{15\pi}{32} c^3 \left[\frac{\langle l^4 \rangle (N^{(q)}/h)}{\langle l \rangle \langle |\boldsymbol{n} \cdot \boldsymbol{q}| \rangle} \right] N_{ij} \tag{45}$$

The choice of either equation (45) or equation (41) depends on the site investigated.

Example

To exemplify the detailed procedure leading to the determination of the crack tensor, a site was chosen for investigation. The site, located near Nakatsugawa, central Japan, is composed of moderately jointed, fresh granite. Joints were surveyed with special emphasis on the following points.

Orientation of joints. Three orthogonal scan lines (EW, NS and vertical) were set on the surface of the granite (25 m × 20 m × 7 m). The strike and the dip were measured whenever the scan lines crossed a joint. The orientation of the joints was shown by plotting their normals as poles on Schmidt's equal area net (Fig. 12). With regard to Fig. 12, joints were classified into three groups (A, B and C). The density function $E(\boldsymbol{n})$ for each group is shown separately in Fig. 13. Using the data of Fig. 13 in equation (34), $N_{ij}^{(A)}$, $N_{ij}^{(B)}$ and $N_{ij}^{(C)}$ were calculated as follows

$$[N_{ij}^{(A)}] = \begin{bmatrix} N_{11} & N_{12} & N_{13} \\ N_{21} & N_{22} & N_{23} \\ N_{31} & N_{32} & N_{33} \end{bmatrix} = \begin{bmatrix} 0{\cdot}135 & -0{\cdot}010 & -0{\cdot}041 \\ -0{\cdot}010 & 0{\cdot}071 & 0{\cdot}078 \\ -0{\cdot}041 & 0{\cdot}078 & 0{\cdot}794 \end{bmatrix}$$

$$[N_{ij}^{(B)}] = \begin{bmatrix} 0{\cdot}789 & 0{\cdot}049 & 0{\cdot}123 \\ 0{\cdot}049 & 0{\cdot}058 & 0{\cdot}011 \\ 0{\cdot}123 & 0{\cdot}011 & 0{\cdot}153 \end{bmatrix} \tag{46}$$

$$[N_{ij}^{(C)}] = \begin{bmatrix} 0{\cdot}031 & -0{\cdot}067 & -0{\cdot}003 \\ -0{\cdot}067 & 0{\cdot}994 & 0{\cdot}080 \\ -0{\cdot}003 & 0{\cdot}080 & 0{\cdot}025 \end{bmatrix}$$

In the calculation, the axes x_1, x_2 and x_3 given in Fig. 12 are referred to.

Trace lengths of joints. Joint traces, which were visible on the horizontal section (25 m × 20 m), were carefully mapped (Fig. 14). Two sets of data were obtained from the map of the joint traces for each group separately. Firstly, a scan line in a direction $\boldsymbol{q}$ was established. The number of cracks crossed by the scan line was counted to give $N^{(q)}/h$, and the correction term $\langle |\boldsymbol{n} \cdot \boldsymbol{q}| \rangle$ was also calculated by using the density function of Fig. 13. Several trials have proved that $(N^{(q)}/h)/\langle |\boldsymbol{n} \cdot \boldsymbol{q}| \rangle$ remains almost constant and does not depend much on the selected direction $\boldsymbol{p}$ of the scan line. Secondly, the frequency distribution diagrams of the trace lengths were prepared (Fig. 15). The joints belonging to group C do not appear on the horizontal map because they are subparallel to the observed plane. So, two large vertical cliffs located near the horizontal section were carefully sketched to provide the same data (Fig. 15). The frequency diagrams are similar in shape but differ in the mean and the standard deviation. This is the main reason that the joints were classified into the three groups. Using these frequency diagrams, the moments of the trace length $\langle l \rangle$ and $\langle l^4 \rangle$ were calculated.

Aperture of joints. Measurements of joint apertures have not been undertaken. Direct observation has shown that the aperture is wider

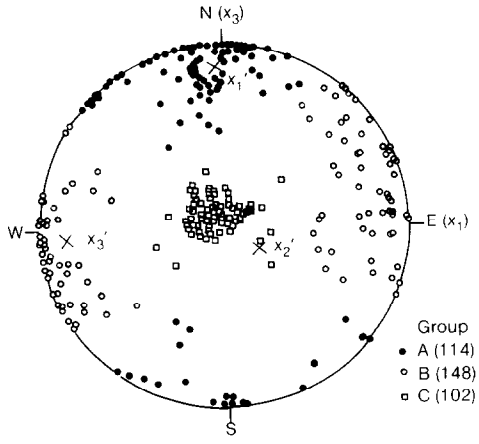

Fig. 12. Schmidt's equal area projection of joints (lower hemisphere projection)

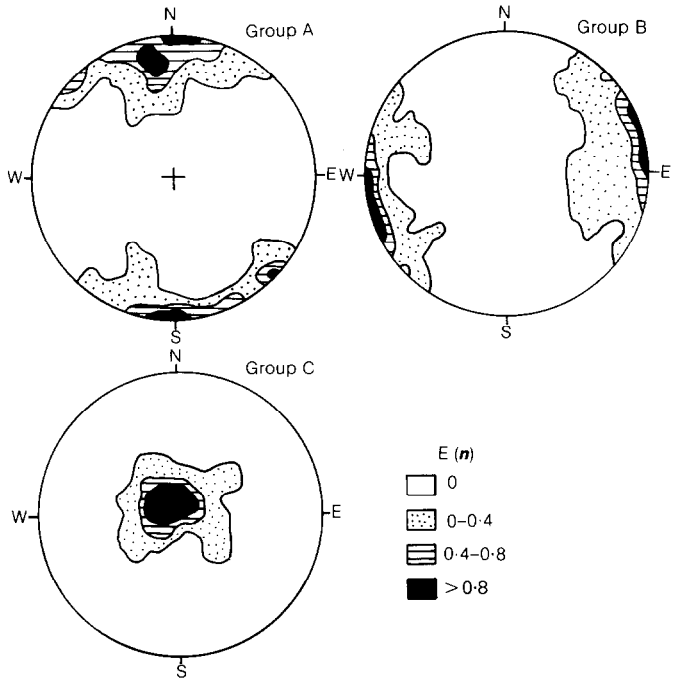

Fig. 13. Estimated density function E(n) for each joint group

with increasing the trace length. This implies that the relation $t = cr$ is preferable to $t = t_0$.

Using all these data in equation (45), the crack tensors $P_{ij}^{(A)}$, $P_{ij}^{(B)}$ and $P_{ij}^{(C)}$ for the groups A, B and C were calculated separately and were summed to give the final crack tensor P_{ij}, as follows

$$[P_{ij}] = [P_{ij}^{(A)}] + [P_{ij}^{(B)}] + [P_{ij}^{(C)}] = c^3 \begin{bmatrix} 186{\cdot}6 & -8{\cdot}3 & -10{\cdot}3 \\ -8{\cdot}3 & 171{\cdot}2 & 60{\cdot}1 \\ -10{\cdot}3 & 60{\cdot}1 & 515{\cdot}0 \end{bmatrix} \quad (47)$$

If the reference axes are selected as the principal axes x_1', x_2' and x_3' of the crack tensor, then equation (47) becomes

$$[P_{ij}] = c^3 \begin{bmatrix} 525{\cdot}6 & 0 & 0 \\ 0 & 187{\cdot}7 & 0 \\ 0 & 0 & 159{\cdot}5 \end{bmatrix} \quad (48)$$

with the principal axes plotted in Fig. 12.

If the crack tensor is substituted in equation (18), the corresponding permeability tensor is obtained. It should be pointed out that it still includes an unknown c, even if the simplification of $\alpha_0 = 0$ and $\lambda = 1/12$ is adopted. Additional information is necessary to complete the theory. Either pressure tests in boreholes or direct measurements of the aperture can provide the necessary information (Bianchi & Snow, 1968; Snow, 1968). It must be emphasized, however, that valuable conclusions have been deduced from equation (13) together with equation (48), i.e.

(a) the degree of anisotropy in hydraulic response of the rock mass
(b) the principal axes of the permeability tensor
(c) the quantitative comparison between rock masses.

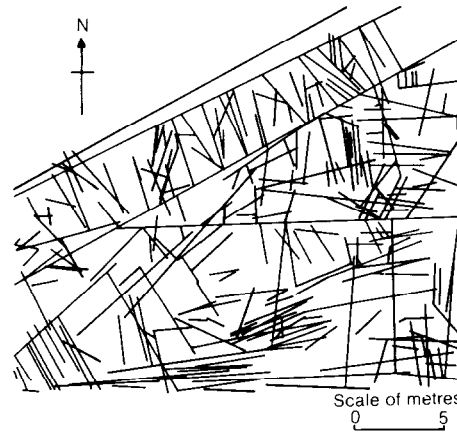

Fig. 14. Map showing joint traces on a horizontal section

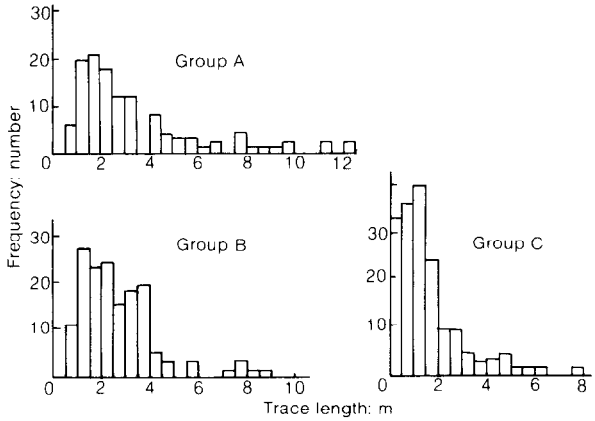

Fig. 15. Frequencies of joint trace lengths (four more joints, 19·3 m, 21·0 m, 23·7 m and 28·8 m in trace length must be added to the diagram for group A)

CONCLUSION

Joints, faults and other geological discontinuities (cracks), which are of widespread occurrence in rock masses, are major flow paths and are much more significant than those in intact rocks. If rock masses contain many cracks, they can be treated as homogeneous, anisotropic porous media. Considering the effect of crack geometry on the permeability tensor, a theory is presented here with the following results.

(*a*) The permeability tensor $k_{ij}^{(c)}$ is concisely expressed by a symmetric, second-rank tensor P_{ij} (called the crack tensor) which depends only on the geometrical properties of related cracks (crack shape, aperture, size and orientation), i.e.

$$k_{ij}^{(c)} = \lambda (P_{kk}\,\delta_{ij} - P_{ij})$$

Here, the constant $\lambda = 1/12$ if the rock mass is fully broken up by many cracks. Otherwise, λ becomes smaller than 1/12, and the crack tensor P_{ij} must be replaced by an effective crack tensor $\bar{P}_{ij}$.

(*b*) The theory leads to the following results which are of great importance in the practical application

- (*i*) the first invariant of $k_{ij}^{(c)}$ is related to the first invariant of P_{ij} with a tangent equal to λ
- (*ii*) the major and minor principal axes of $k_{ij}^{(c)}$ accord with the minor and major principal axes of P_{ij} respectively
- (*iii*) the results are well supported by the numerical analyses on the permeability of cracked media.

(*c*) A stereological interpretation is very useful for estimating the crack tensor from in situ measurable quantities. Crack orientation data presented on Schmidt's net together with mapping of crack traces that are visible on exposures are used to provide the crack tensor for a moderately jointed granite. The following valuable information is derived from the tensor: the degree of anisotropy in hydraulic response of rock masses, the principal axes of the permeability tensor and a quantitative comparison between rock masses.

ACKNOWLEDGEMENTS

The Author wishes to express his gratitude to Mr Maeshibu, Mr Hatsuyama and Mr Suno for their assistance in joint surveys in the field.

REFERENCES

Bear, J. (1972). *Dynamics of fluids in porous media.* New York: Elsevier.

Bianchi, L. & Snow, D. T. (1968). Permeability of crystalline rock interpreted from measured orientations and apertures of fractures. *Ann. Arid Zone* **8,** No. 2, 231–245.

Brace, W. F. (1980). Permeability of crystalline and argillaceous rocks. *Int. J. Rock Mech. Min. Sci. Geomech. Abstr.* **17,** 241–251.

Caldwell, J. A. (1972). The theoretical determination of the permeability tensor for jointed rock. *Symp. Percolation Through Fissured Rock. Stuttgart*: International Society for Rock Mechanics and International Association of Engineering Geology.

Dienes, J. K. (1982). Permeability, percolation and statistical crack mechanics. *23rd Symp. on Rock Mech., Berkeley.*

Hoek, E. & Brown, E. T. (1980). *Underground excavation in rock.* London: Institution of Mining and Metallurgy.

Hudson, J. A. & Pointe, P. R. (1980). Printed circuits

for studying rock mass permeability. *Int. J. Rock Mech. Min. Sci. Geomech. Abstr.* **17,** 297–301.
Kanatani, K. (1984). Distribution of directional data and fabric tensors. *Int. J. Engng Sci.* **22,** No. 2, 149–164.
Kendall, M. G. & Moran, P. A. P. (1963). *Geometrical probability.* New York: Hafner.
Long, J. C. S., Remer, J. S., Wilson, C. R. & Witherspoon, P. A. (1982). Porous media equivalents for networks of discontinuous fractures. *Wat. Resour. Res.* **18,** No. 3, 645–658.
Müller, L. (1964). The rock slide in the Vajont valley. *Rock Mech. Engng Geol.* **6,** 1–91.
Oda, M. (1983). A method for evaluating the effect of crack geometry on the mechanical behavior of cracked rock masses. *Mech. Mater.* **2,** 163–171.
Oda, M. (1984). Similarity rule of crack geometry in statistically homogeneous rock masses. *Mech. Mater.* **3,** 119–129.
Parsons, R. W. (1966). Permeability of idealized fractured rock. *Soc. Petrol. Engng J.* **10,** 126–136.
Robertson, A. (1970). The interpretation of geological factors for use in slope stability. *Proc. Symp. Theoretical Background to the Planning of Open Pit Mines with Special Reference to Slope Stability,* pp. 55–71.
Scheidegger, A. E. (1957). *The physics of flow through porous media.* University of Toronto Press.
Snow, D. T. (1968). Rock fracture spacings, openings, and porosities. *J. Soil Mech. Fdns Div. Am. Soc. Civ. Engrs* **94,** SM1, 73–91.
Snow, D. T. (1969). Anisotropic permeability of fractured media. *Wat. Resour. Res.* **5,** No. 6, 1273–1289.
Turner, F. J. & Weiss, L. E. (1963). *Structural analysis of metamorphic tectonites.* New York: McGraw-Hill.
Witherspoon, P. A., Wang, J. S. Y., Imai, K. & Gale, J. E. (1980). Validity of cubic law for fluid flow in a deformable rock fracture. *Wat. Resour. Res.* **16,** No. 6, 1016–1024.

APPENDIX 1

The entire solid angle Ω corresponds to a surface of a unit sphere and equals 4π. It can be divided into m pieces with the same area $\Delta\Omega$

$$\Omega = \sum_{i=1}^{m} \Delta\Omega^{(i)} = 4\pi \tag{49}$$

($\Delta\Omega = \Delta\Omega^{(i)}$) where the superscript i denotes an ith piece. Using the probability density $E(\boldsymbol{n})$, the number $\Delta M^{(i)}$ of the normal $\boldsymbol{n}$ vectors oriented inside the ith small solid angle $\Delta\Omega^{(i)}$ is given by

$$\Delta M^{(i)} = 2N E^{(i)}(\boldsymbol{n})\, \Delta\Omega^{(i)} \tag{50}$$

where

$$2N = \sum_{i=1}^{m} \Delta M^{(i)} \tag{51}$$

If m is selected as 200, each $\Delta\Omega^{(i)}$ becomes $4\pi/200$. Then equation (50) can be rewritten as

$$4\pi E^{(i)}(\boldsymbol{n}) = \frac{\Delta M^{(i)}}{N} \times 100 \tag{52}$$

It should be noted that $\Delta M^{(i)}$ merely corresponds to the number of normal vectors per unit per cent area ($4\pi/200$) counted on the Schmidt net. Accordingly, the right-hand side is the percentage concentration of $\boldsymbol{n}$ vectors per unit per cent area. Now, it is clear that $E(\boldsymbol{n})$ is determined by the percentage concentration of $\boldsymbol{n}$ vectors per unit per cent area divided by 4π.